PAPER

Epoxy composites with functionalized molybdenum disulfide nanoplatelet additives

Ming Zhao,[ab] Lizhu Liu, [ID] *[ac] Bin Zhang,*[b] Mingming Sun,[b] Xugang Zhang,[b] Xue Zhang,[b] Jianhui Li[b] and Lei Wang[b]

As a typical layered inorganic analogue of graphene, molybdenum disulfide (MoS_2) has gained intensive attention and become a research hotspot due to its unique two dimensional nanostructure and excellent properties. The enhancement in the thermal and mechanical properties of polymer/inorganic nanosheet composites depends strongly on their interfacial interaction. In this study, we exfoliated bulk MoS_2 into nanosheets which were subsequently functionalized using 3-mercaptopropyltriethoxysilane. The functionalized MoS_2 (f-MoS_2) were dispersed in epoxy polymers at loading fractions of up to 1% by weight *via* ultrasonication and three roll mills. We characterized the tensile, fracture and adhesive properties of the composite and show that f-MoS_2 nanoplatelets are highly effective at enhancing the mechanical properties of the epoxy at very low nanofiller loading fractions (0.1–0.7% by weight). Our results show the potential of functionalized 2D sheets of transition metal dichalcogenides as reinforcing additives in polymeric composites. The results indicate that the glass transition temperature increases significantly for the lower weight fraction composites, from 135 °C for the baseline (unfilled) epoxy to 146 °C at 0.7% f-MoS_2 loading. The apparent shear strength at 120 °C increases significantly for the lower weight fraction composites, from 13.8 MPa for the baseline (unfilled) epoxy to 24.9 MPa at 0.7% f-MoS_2 loading.

1. Introduction

Over the past few years there has been great interest in trying to reinforce polymer materials with nanoscale fillers to improve their electronic, mechanical, optical, flexible and thermal properties[1–4] for a variety of engineering applications.[5–8] Two-dimensional (2D) layered nanomaterials exfoliated from bulk layered inorganic compounds,[9–12] such as graphene, molybdenum disulfide (MoS_2) and tungsten disulfide (WS_2), have motivated great attention owing to their applicability in fields ranging from catalysis,[13] lubricants,[14] super capacitors,[15–17] transistors[18] and cathode materials for lithium batteries to biomedicine.[19] As high band gap semiconductors, transition metal dichalcogenides (TMDCs) will not impart electrical conductivity to the polymer matrix while at the same time potentially improving mechanical properties such as elastic modulus, strength, toughness, wear, creep and fatigue resistance.[20,21] As is well known, the properties of inorganic nano-fillers/polymer composites depend strongly on two factors: one is the interaction between the nano-fillers and the polymer matrix; the other is the dispersion state of nano-fillers in the polymer matrix.[22,23] The exfoliation degree of bulk MoS_2 is very important to fabricate its polymer nanocomposites with effective reinforcement. The layered structure of MoS_2 enables easy intercalation of lithium ions (Li^+). It is convenient to prepare the polymer nanocomposites by the intercalation of Li^+ and then exfoliation to a single or few layers through the hydrolysis of the Li^+.[24,25] Therefore, most of the MoS_2/polymer composites are focused on water-soluble polymers such as poly(vinyl alcohol),[26] poly(ethylene oxide),[27] and chitosan,[28] prepared through a solution blending method.

In this study, we exfoliated bulk MoS_2 into nanosheets which was subsequently functionalized using 3-mercaptopropyltriethoxysilane. We characterized the tensile and fracture and adhesive properties of the composite and show that f-MoS_2 nanoplatelets are highly effective at enhancing the mechanical properties of the epoxy at very low nanofiller loading fractions.

[a]School of Materials Science and Engineering, Harbin University of Science and Technology, 4 Linyuan Road, Harbin, Heilongjiang 150040, P. R. China. E-mail: liulizhu_hust@163.com

[b]Institute of Petrochemistry Heilongjiang Academy of Sciences, 164 Zhongshan Road, Harbin, Heilongjiang 150040, P. R. China. E-mail: zhangbin_hipc@126.com

[c]Key Laboratory of Engineering Dielectrics and Its Application, Ministry of Education, Harbin University of Science and Technology, 52 Xuefu Road, Harbin, Heilongjiang 150080, P. R. China

2. Experimental

2.1 Materials

Molybdenum disulfide, *n*-hexane and tetrahydrofuran were purchased from Sinopharm Chemical Reagent Co., Ltd.
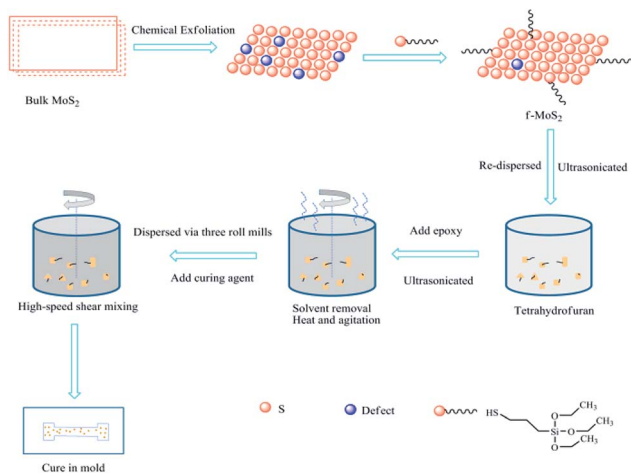
Scheme 1 Schematic illustration of f-MoS$_2$/epoxy composite preparation route.

(China). The *n*-butyl lithium (2.2 M in hexane) was purchased from Alfa Aesar without further purification. Diglycidyl ether of Bisphenol-F type epoxy resin (NPEF-170) were purchased from Nan Ya Plastics Corporation. 3,3′-Dimethyl-4,4′-diamino-dicyclohexylmethane (DMDC) were purchased from BASF. 3-Mercaptopropyltriethoxysilane (KH580) were purchased from Nanjing Shuguang Chemical Group Co., Ltd. Deionized water is used for all experiments unless otherwise stated.

2.2 Synthesis of functionalized MoS$_2$ nanosheets

Li$_x$MoS$_2$ was prepared by the solvothermal methodology, similar to the preparation procedure of Li$_x$WS$_2$. In a typical experiment, 1.0 g bulk MoS$_2$ powder was soaked in the autoclave and 36 mL 0.5 M solution of *n*-butyl lithium in hexane was then added. The autoclave was tightly sealed and heated at 90 °C for 4 h. Following the intercalation by lithium, the MoS$_2$ sample was filtered and washed with anhydrous hexane, and then dried at 50 °C in vacuum oven. Exfoliation of MoS$_2$ into nanosheets was achieved *via* the rapid hydrolysis and ultra-sonication of Li$_x$MoS$_2$. In a typical reaction, 0.5 g Li$_x$MoS$_2$ was hydrolysed in 1 L water, and ultrasonicated at ambient temperature for 4 h to produce a colloidal suspension of MoS$_2$ nanosheets. For the functionalization of MoS$_2$ nanosheets, 1.0 g of KH580 was added into 0.25 g of MoS$_2$ nanosheets dispersed in 500 mL of water. After sonication for 20 min and stirring overnight, excess KH580 was removed by filtration followed by several times of water washing. The obtained f-MoS$_2$ was dried in a vacuum oven at 50 °C for 12 hours.

2.3 Preparation of f-MoS$_2$/epoxy nanocomposites

Scheme 1 illustrates the procedure for preparing f-MoS$_2$/epoxy nanocomposites. The f-MoS$_2$/epoxy nanocomposites were prepared by the solvent blending method and grinding method, maintaining the nanofiller loading at 0.1 wt%, 0.3 wt%, 0.5 wt%, 0.7 wt% and 1 wt%, respectively. First, the calculated f-MoS$_2$ nanosheets were re-dispersed in tetrahydrofuran and
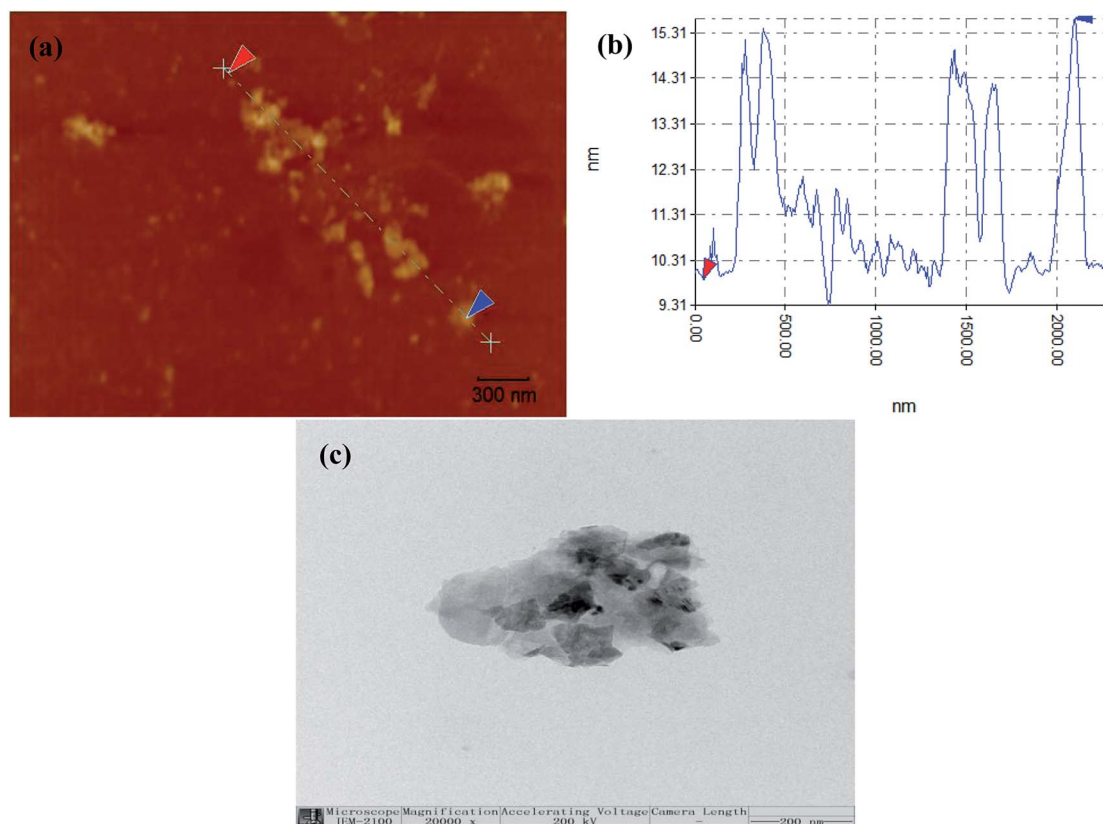

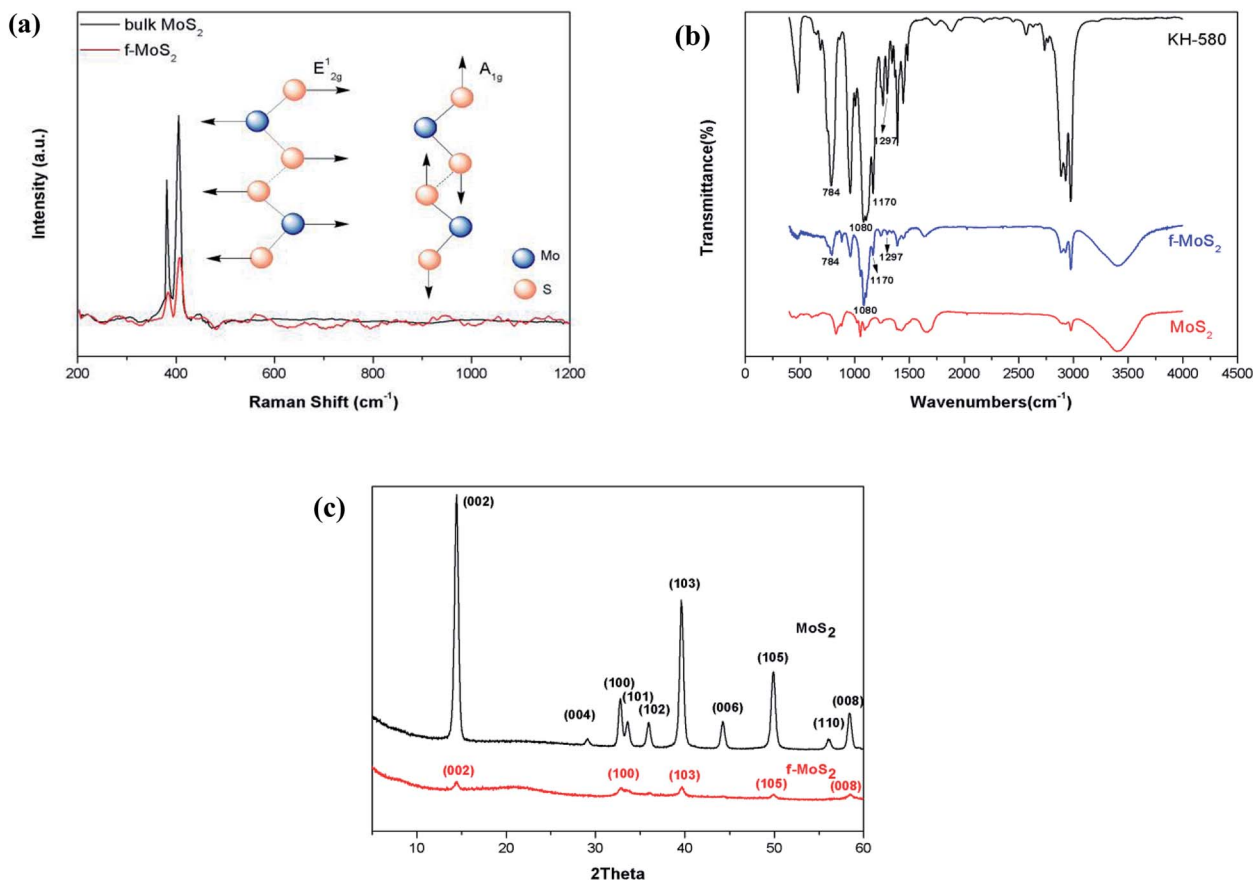**Fig. 1** AFM images (a) and thickness profiles (b) of f-MoS$_2$ nanosheets; TEM images of f-MoS$_2$ (c).

Fig. 2 (a) Raman spectrum of bulk MoS$_2$ and f-MoS$_2$ nanosheets; (b) Fourier transform infrared spectra of KH580, MoS$_2$ and f-MoS$_2$; (c) Powder X-ray diffraction patterns of MoS$_2$ and f-MoS$_2$.

ultrasonicated at ambient temperature for 4 h. The epoxy resin was then added into the aforementioned dispersion and stirred under ultrasonic agitation for 6 h. The solvent was gradually removed through heating the mixture on a magnetic hot plate with stirring. After the f-MoS$_2$/epoxy mixture had cooled to room temperature, the mixture was grinded 3 times by three roll mills. Subsequently, a low-viscosity curing agent (DMDC) was added, and a planetary vacuum mixer (ARV-310, Thinky) was used to blend the f-MoS$_2$/epoxy slurry in a vacuum environment for 4 min at 1800 rpm. Finally, Teflon molds were used to cure the nanocomposite samples, cured for 2 h at 80 °C and post cured for 2 h at 150 °C.

2.4   Characterization

Transmission electron microscopy (TEM; JEM-2100, Japan Electron Optics Laboratory Co., Ltd.) was used to investigate the morphologies of the exfoliated f-MoS$_2$ nanosheets. Atomic force microscopy (AFM) images of f-MoS$_2$ were obtained using a Being Nano-Instruments CSPM5500 in the tapping mode. The powder X-ray diffraction (XRD) patterns were recorded with a XRD-7000 Shimadzu X-ray diffractometer (Cu Kα a radiation and λ = 0.1542 nm), operating at 40 kV voltage and 30 mA current. Laser Raman spectroscopy measurements were performed using a XploRA PLUS Raman microscope (HORIBA Scientific) with an excitation provided in back-scattering geometry by a 532 nm argon laser line. Fourier transform infrared (FTIR) spectra were recorded on a BRUKER TENSOR27 FTIR spectrometer using the KBr disc method. All the samples were analyzed with the transmission mode and the wavenumber range was set from 400 to 4000 cm^{-1}. Dynamic mechanical analysis (DMA) was performed using a DMA Q800 apparatus (TA Instruments Inc.) at a fixed frequency of 1 Hz in the temperature range from room temperature to 200 °C at a linear heating rate of 5 °C min^{-1}. Morphology of the sample after being gold-sputtered was studied by a JEOL JSM-IT300 scanning electron microscope (SEM). The specimens of nanocomposites were cryogenically fractured in liquid nitrogen first and then sputter-coated with a conductive layer. Energy dispersive X-ray analysis (EDAX) was performed using a AMETEK ELEMENT. Static tensile loading tests (the thickness is 3.2 ± 0.4 mm; The width is 10 ± 0.2 mm) and apparent shear strength tests (the thickness of the sheets is 1.62 ± 0.125 mm; the length of overlap is 12.7 ± 0.25 mm) were performed using an Instron 5982 universal testing system following the ASTM D638 standard and the ASTM D1002 standard, respectively. Impact resistance tests (sample size 80 ± 2 mm × 10 ± 0.5 mm × 4 ± 0.2 mm) were conducted using a PTM1000 material testing system (SHENZHEN SUNS TECHNOLOGY STOCK CO., LTD.) following the ISO 179 standard. Five parallels for each sample were tested and the average value was reported.
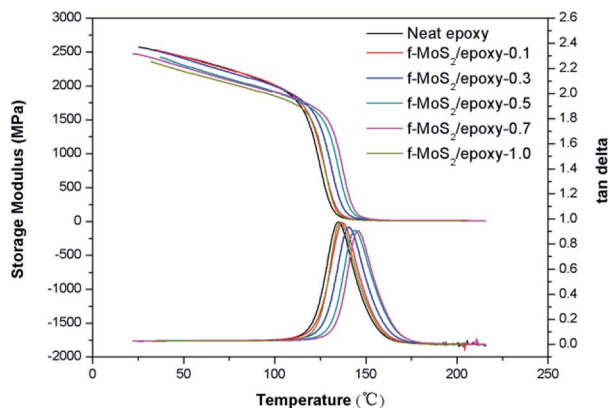
Fig. 3 Plots of storage modulus and tan delta *versus* temperature for neat epoxy and f-MoS$_2$/epoxy composites.

3.   Results and discussion

3.1   Characterization of MoS$_2$ nanosheets

To determine the average f-MoS$_2$ nanosheets thickness, we performed atomic force microscopy (AFM) scans as shown in Fig. 1a and b. The thickness of the f-MoS$_2$ nanosheets ranges from 1 to 6 nm, while the average thickness of the monolayer

MoS$_2$ is about 1 nm according to the previous reports.[29,30] This indicates that the f-MoS$_2$ nanosheets in our study is composed of 1–6 layers of MoS$_2$. The morphologies of f-MoS$_2$ nanosheets (Fig. 1c) were investigated by TEM. The lateral dimensions of f-MoS$_2$ nanosheets is about 300–500 nm.

Raman spectra of the bulk MoS$_2$ (Fig. 2a) shows modes at 380.9 cm^{-1} (the E$_{2g}^1$ mode corresponding to in-plane vibrations) and at 408.6 cm^{-1} (the A$_{1g}$ mode that corresponds to out-of-plane vibrations) which are characteristic modes of the trigonal prismatic structure of MoS$_2$. For f-MoS$_2$, the E$_{2g}^1$ peak shifts to a higher frequency and the A$_{1g}$ peaks of MoS$_2$ is transferred to a lower frequency, indicating that f-MoS$_2$ are thinner than bulk MoS$_2$.[31–35]

To determine the conjugation of KH580 and MoS$_2$, Fourier transform infrared (FTIR) spectra were recorded as shown in Fig. 2b. Compared to pristine MoS$_2$, the spectra of f-MoS$_2$ exhibit characteristic absorption bands at 1297, 1170, 1080 and 784 cm^{-1} which are attributed to the stretching vibration of C–S, C–C, Si–O and Si–C, respectively. These characteristic bands originate from KH580, which confirms the functionalization of KH580 on the MoS$_2$.

Fig. 2c shows the powder XRD profiles of bulk MoS$_2$ and f-MoS$_2$. The diffraction pattern of bulk MoS$_2$ showed intense and
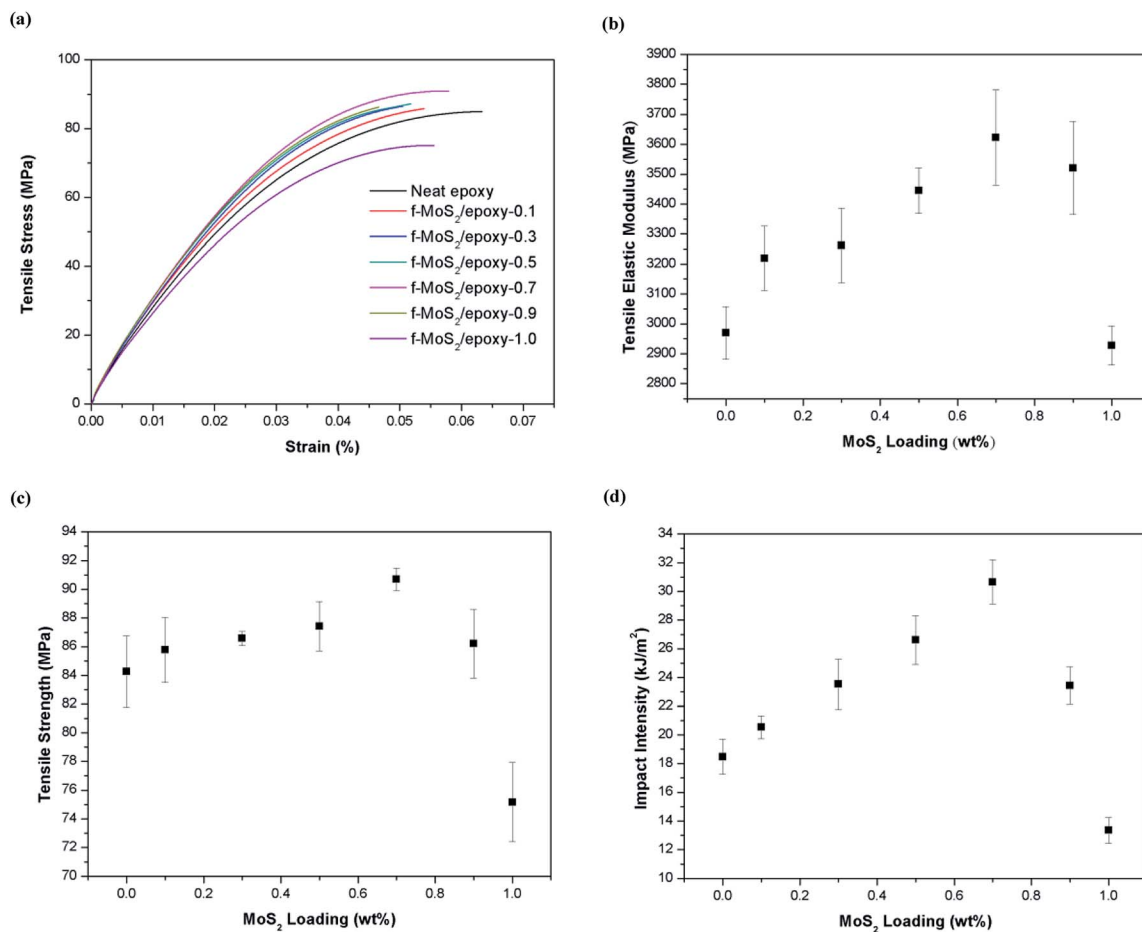

Fig. 4   (a) Stress–strain curves of neat epoxy and f-MoS$_2$/epoxy nanocomposites with various loadings of f-MoS$_2$; (b) Young's modulus *vs.* f-MoS$_2$ nanosheets loading fraction; (c) ultimate tensile strength *vs.* f-MoS$_2$ nanosheets loading fraction; (d) impact intensity *vs.* f-MoS$_2$ nanosheets loading fraction.
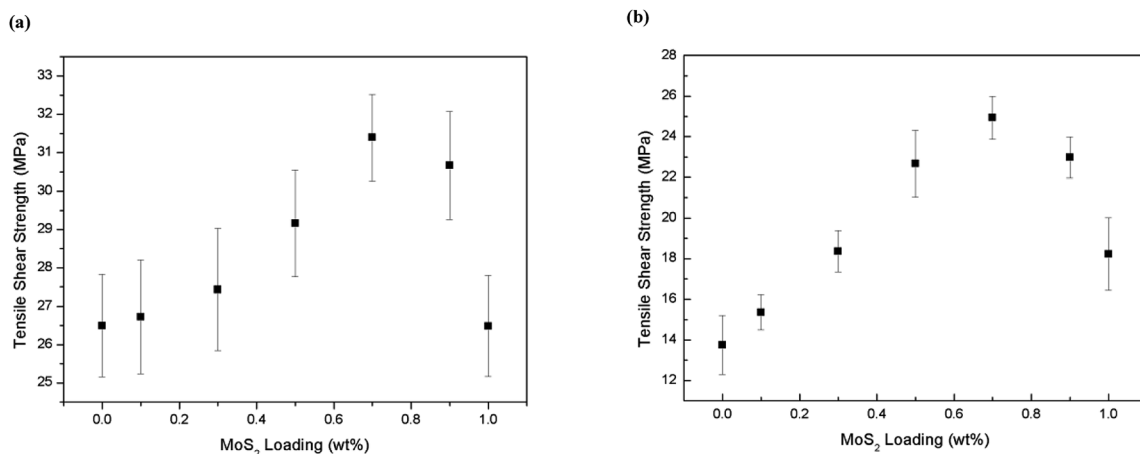
Fig. 5 (a) Apparent shear strength at room temperature *vs.* f–MoS$_2$ nanosheets loading fraction; (b) apparent shear strength at 120 °C *vs.* f–MoS$_2$ nanosheets loading fraction.

sharp peaks at 14.48, 32.78, 39.76, 49.96, and 56.32 (2 theta), which correspond to the (002), (100), (103), (105), and (110) planes, respectively. All the characteristics bands of bulk MoS$_2$ correspond well with the previous report. Post functionalization, the peaks corresponding to the (004), and (006) planes have disappeared. The (002) diffraction peak is still present at 14.4 for f-MoS$_2$, although the intensity of the peak has notably decreased. Low intensity peaks corresponding to the (100), (103), (105) and (008) planes can also be observed for f-MoS$_2$. These features are in good agreement with disordered restacking of the exfoliated sheets during the drying process.

Additionally, the high quality exfoliated MoS$_2$ nanosheets reported by predecessors still displayed prominent diffraction peaks.[36]

The influence of MoS$_2$ and f-MoS$_2$ on the dynamic mechanical thermal behaviors of the epoxy composites was investigated by DMA. Storage modulus curves and loss angle tangent of epoxy and its nanocomposites are presented in Fig. 3. The storage modulus is a measure of the stiffness, the storage modulus (E') of the f-MoS$_2$/epoxy composites decreased with the increase of the f-MoS$_2$ loading. In the case of f-MoS$_2$/epoxy-1.0, the storage modulus was about 7.31% lower than that of neat
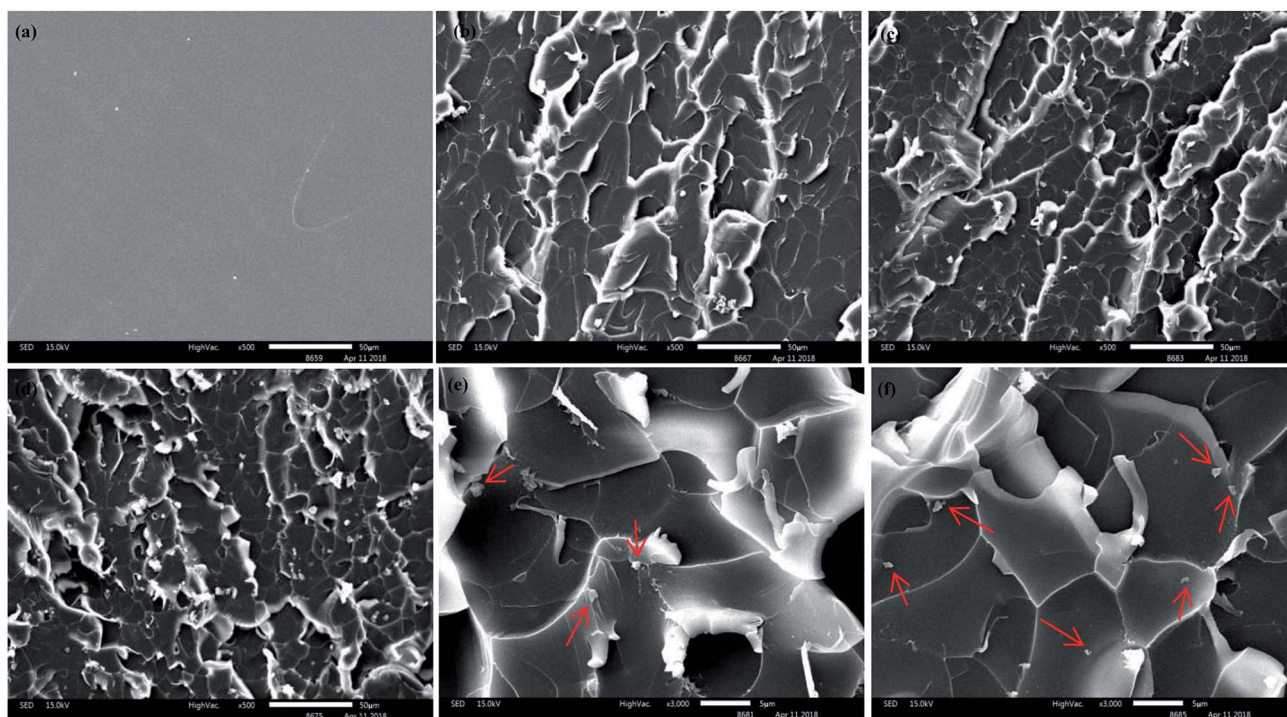

Fig. 6 Scanning electron microscopy images of the fracture surfaces of neat EP (a), 0.3 wt% f-MoS$_2$/epoxy (b), 0.7 wt% f-MoS$_2$/epoxy (c and e) and 1.0 wt% f-MoS$_2$/epoxy (d and f) nanocomposites.
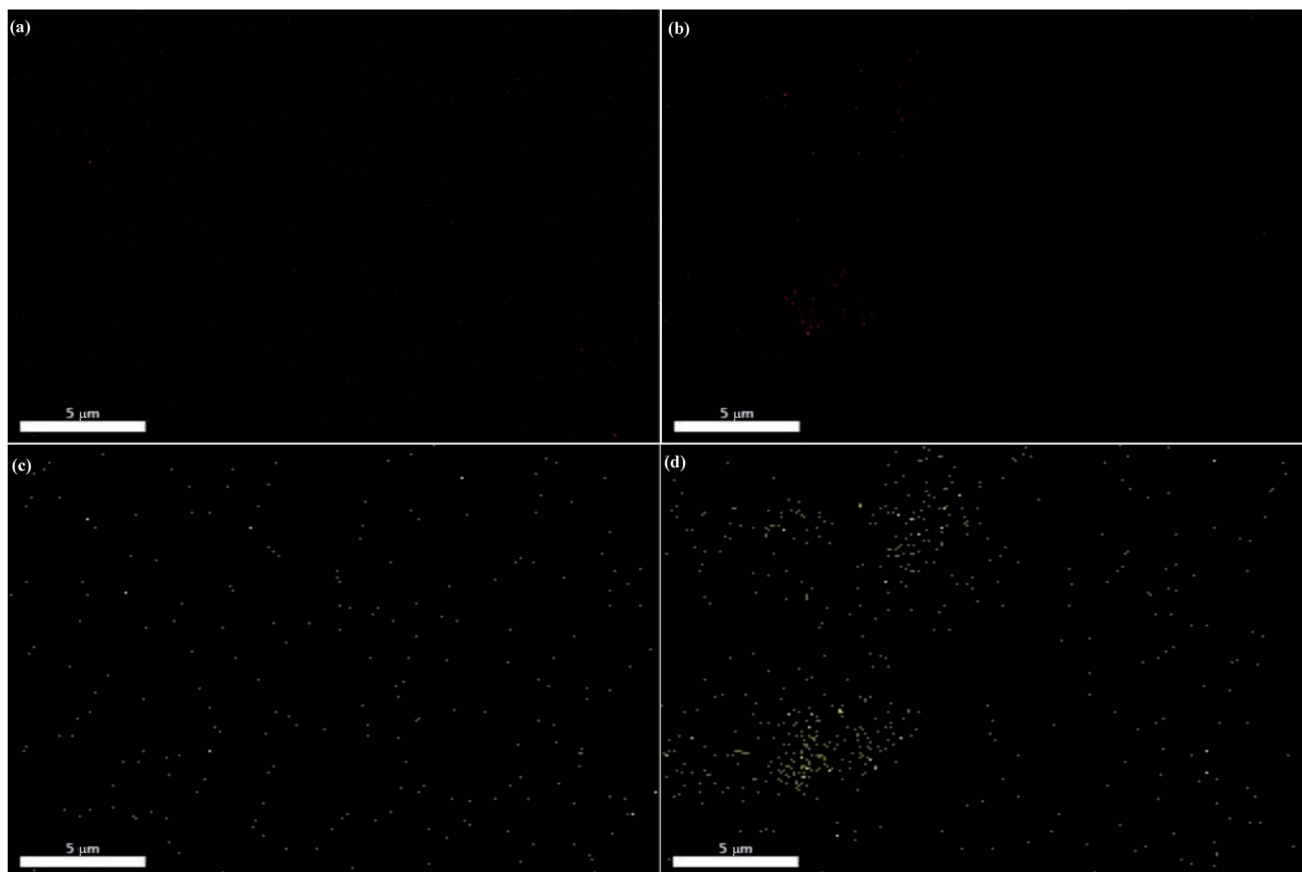
Fig. 7 Energy dispersive X-ray analysis images of the molybdenum element distribution mapping of 0.7 wt% f-MoS$_2$/epoxy (a) and 0.7 wt% bulk MoS$_2$/epoxy (b) nanocomposites, the sulfur element distribution mapping of 0.7 wt% f-MoS$_2$/epoxy (c) and 0.7 wt% bulk MoS$_2$/epoxy (d) nanocomposites.

epoxy at 35 °C. Moreover, E' was generally decreased by the addition of f-MoS$_2$ in all temperature ranges. Incorporation of nanofillers into a polymer matrix can also affect its glass transition temperature (T_g). The glass transition temperature is determined by the peak of tan delta curves. The results indicate that the T_g increases significantly for the lower weight fraction composites, from 135 °C for the baseline (unfilled) epoxy to 146 °C at 0.7% f-MoS$_2$ loading. For the higher weight loadings up to 1.0%, the T_g decreases to approximately that of the neat epoxy. Since the T_g is a thermal transition where polymer chain motion significantly increases, the increased T_g for the low weight fraction f-MoS$_2$ nanocomposites is indicative of decreased chain mobility caused by interfacial interactions between the epoxy chains and the surfaces of the well dispersed f-MoS$_2$ nanoplatelets additives.[37,38] Conversely, at the higher loading fractions, the f-MoS$_2$ nanoplatelets will likely form agglomerates, resulting in fewer interfacial interactions and the matrix mobility therefore returns toward the value of the neat epoxy.[39] The trend seen in the T_g response (Fig. 3) corresponds well to those seen for the high temperature apparent shear strength (Fig. 5b).

The typical stress–strain curves of the baseline epoxy and f-MoS$_2$/epoxy nanocomposites are shown in Fig. 4a. Fig. 4b compares the Young's modulus of the pristine epoxy and the

nanocomposite samples, and Fig. 4c shows their ultimate tensile strength. The error bars represent the maximum and minimum values obtained. The results indicate that f-MoS$_2$ nanosheets are effective at increasing the elastic modulus and the tensile strength of the epoxy at small nanosheets loadings (0.1–0.7% by weight). The tensile modulus of MoS$_2$/epoxy composites increased from 2.97 to 3.62 GPa (approximately a 22% increase over neat epoxy), and the tensile strength increased from 84.3 to 90.7 MPa (approximately a 8% increase over neat epoxy) when the MoS$_2$ content increased from 0 to 0.7%. Moreover, as the MoS$_2$ content increased from 0.7 to 1%, the tensile modulus and tensile strength reduced to 2.93 GPa and 75.2 MPa, respectively.[40–42] There ported results are the average of 5 different tests for each f-MoS$_2$ nanosheets loading fraction.

As can be seen, the addition of f-MoS$_2$ nanosheets significantly improves the impact intensity of the epoxy matrix (Fig. 4d). It is strongly evident that even a small amount of f-MoS$_2$ nanosheets could significantly improve the mechanical strength. The maximum increase in impact intensity is 66% in the sample of f-MoS$_2$/epoxy-0.7. However, beyond 0.7% loading there is a reduction in performance and at 1.0% loading the impact intensity of the nanocomposite sample reduced to 13.3 kJ m^{-2}.

The reinforcing effects of the f-MoS$_2$ on the adhesive properties of the epoxy composites are summarized in Fig. 5a and b. The apparent shear strength of f-MoS$_2$/epoxy composites at room temperature increased from 26.5 to 31.4 MPa (approximately an 18% increase over neat epoxy), and the tensile shear strength at 120 °C increased from 13.8 to 24.9 MPa (approximately an 80% increase over neat epoxy) when the f-MoS$_2$ nanosheets content increased from 0 to 0.7%. However, beyond 0.7% loading there is a reduction in performance at room temperature and at 1% loading the performance of the nanocomposite sample is comparable to the baseline epoxy.[43,44]

Moreover, as the f-MoS$_2$ nanosheets content increased from 0.7 to 0.9 and 1.0 wt%, the apparent shear strength of the f-MoS$_2$/epoxy composites at 120 °C turned to 22.9 and 18.2 MPa, respectively, but a reducing trend was observed on the apparent shear strength of the f-MoS$_2$/epoxy composites at 120 °C.

To understand the dispersion levels of and f-MoS$_2$ in epoxy resin, the freeze-fractured surface microstructures (Fig. 6a–f) of epoxy nanocomposites were investigated by SEM. According to the previous studies, the fracture roughness of the polymer nanocomposites reflects the dispersion level and interfacial interaction to some degree.[45,46] It can be observed in Fig. 6a that the neat epoxy displays a smooth fracture surface. It is clear that the fracture surface roughness of the f-MoS$_2$/epoxy nanocomposites increase with increasing addition of f-MoS$_2$.[47–49] In addition, it is observed that numerous MoS$_2$ agglomerates are pulled out of 1.0 wt% f-MoS$_2$/epoxy nanocomposite. Nevertheless, few MoS$_2$ agglomerates emerge in the SEM images of 0.7 wt% f-MoS$_2$/epoxy nanocomposite because most of the f-MoS$_2$ nanosheets are uniformly embedded into the EP matrix.

To further verify the dispersion states of bulk MoS$_2$ and f-MoS$_2$ in an epoxy matrix, the molybdenum and sulfur element distribution mapping of the bulk MoS$_2$/epoxy-0.7 and f-MoS$_2$/epoxy-0.7 is provided in Fig. 7. In short, f-MoS$_2$ nanosheets exhibit better dispersion in the epoxy matrix and compatibility with the matrix than those of bulk MoS$_2$ because of the thinner structure and stronger interfacial interaction.[50,51] Undoubtedly, the resultant homogeneous dispersion of f-MoS$_2$ sheets in nanocomposites is beneficial to their reinforced performances.

Based on the results aforementioned, the high-efficiency reinforcement might be probably attributed to the uniform dispersion of the f-MoS$_2$ in the epoxy matrix (as observed in the EDAX images of Fig. 7a and c), as well as to the formation of strong interactive interfaces between f-MoS$_2$ and the epoxy matrix (as indicated in the SEM images of Fig. 6b–f). In the case of f-MoS$_2$/epoxy nanocomposites, the exfoliated f-MoS$_2$ nanosheets with a high elastic modulus served as the reinforcement rather than the bulk MoS$_2$ particles. The polymer chains adsorbed on the nanosheet surfaces are substantial due to the strong interfacial interactions, which increased the effective volume fraction of the reinforcement. The expansion of the effective volume fraction is presented to the continuous phase with consequences for adsorption and immobilization,[52,53] which provided a high capacity for transferring the stress from the epoxy matrix to f-MoS$_2$ nanosheets.

4. Conclusions

In summary, functionalized MoS$_2$ nanosheets were synthesized from bulk MoS$_2$ via chemical exfoliation and subsequent surface modification with 3-mercaptopropyltriethoxysilane. The functionalized MoS$_2$ were dispersed in epoxy polymers at loading fractions of up to wt 1% by ultrasonication and three roll mills. The dispersion states of f-MoS$_2$ in an epoxy matrix was much better than bulk MoS$_2$ by EDAX and SEM. With only 0.7 wt% of f-MoS$_2$, a 22% increase in tensile elastic modulus, a 66% increase in impact intensity, an 80% increase in tensile shear strength at 120 °C and an 11 °C increment in glass transition temperature of the resultant f-MoS$_2$/epoxy nanocomposite were attained. The superior reinforcing efficiency of f-MoS$_2$ can be attributed to the good dispersion of MoS$_2$ sheets and the strong interfacial interaction with the polymer matrix enabled by surface functionalization of MoS$_2$.

Conflicts of interest

There are no conflicts to declare.

Notes and references

1 X. Zhang, O. Alloul, Q. L. He, J. H. Zhu, M. J. Verde, Y. T. Li, S. Y. Wei and Z. H. Guo, Strengthened magnetic epoxy nanocomposites with protruding nanoparticles on the graphene nanosheets, *Polymer*, 2013, **54**, 3594–3604.

2 O. Eksik, J. Gao, S. A. Shojaee, A. Thomas, P. Chow, S. F. Bartolucci, D. A. Lucca and N. Koratkar, Epoxy nanocomposites with two-dimensional transition metal dichalcogenide additives, *ACS Nano*, 2014, **8**, 5282–5289.

3 W. L. Song, P. Wang, L. Cao, A. Anderson, M. J. Meziani, A. J. Farr and Y. P. Sun, Polymer/boron nitride nanocomposite materials for superior thermal transport performance, *Angew. Chem., Int. Ed.*, 2012, **51**, 6498–6501.

4 S. P. Pang, H. N. Tsao, X. L. Feng and K. Mullen, Patterned graphene electrodes from solution-processed graphite oxide films for organic field-effect transistors, *Adv. Mater.*, 2009, **21**, 3488–3491.

5 S. Stankovich, D. A. Dikin, G. H. B. Dommett, K. M. Kohlhaas, E. J. Zimney, E. A. Stach, R. D. Piner, S. T. Nguyen and R. S. Ruoff, Graphene-based composite materials, *Nature*, 2006, **442**, 282–286.

6 H. Kim, A. A. Abdala, C. W. Macosko and W. M. Christopher, Graphene/polymer nanocomposites, *Macromolecules*, 2010, **43**, 6515–6530.

7 A. Splendiani, L. Sun, Y. B. Zhang, T. S. Li, J. Kim, C. Y. Chim, G. Galli and F. Wang, Emerging photoluminescence in monolayer MoS$_2$, *Nano Lett.*, 2010, **10**, 1271–1275.

8 K. Watanabe, T. Taniguchi and H. Kanda, Direct-bandgap properties and evidence for ultraviolet lasing of hexagonal boron nitride single crystal, *Nat. Mater.*, 2004, **3**, 404–409.

9 J. N. Coleman, M. Lotya, A. O'Neill, S. D. Bergin, P. J. King, U. Khan and K. Young, Two-dimensional nanosheets produced by liquid exfoliation of layered materials, *Science*, 2011, **331**, 568–571.

10 V. Nicolosi, M. Chhowalla, M. G. Kanatzidis, M. S. Strano and J. N. Coleman, Liquid exfoliation of layered materials, *Science*, 2013, **340**, 1226419.

11 Z. Liu, L. Zhang, R. Wang, S. Poyraz, J. Cook, M. Bozack, S. Das, X. Zhang and L. Hu, Ultrafast microwave nano-manufacturing of fullerene-like metal chalcogenides, *Sci. Rep.*, 2016, **6**, 22503.

12 L. Zhang, W. Du, A. Nautiyal, Z. Liu and X. Zhang, Recent progress on nanostructured conducting polymers and composites: synthesis, application and future aspects, *Sci. China Mater.*, 2018, **61**, 303.

13 R. R. Chianelli, M. H. Siadati, M. P. D. Rosa, G. Berhault, J. P. Wilcoxon, R. Bearden and B. L. Abrams, Catalytic properties of single layers of transition metal sulfide catalytic materials, *Catal. Rev.: Sci. Eng.*, 2006, **48**, 1–41.

14 T. Polcar and A. Cavaleiro, Review on self-lubricant transition metal dichalcogenide nanocomposite coatings alloyed with carbon, *Surf. Coat. Technol.*, 2011, **206**, 686–695.

15 J. M. Soon and K. P. Loh, Electrochemical double-layer capacitance of MoS_2 nanowall films, *Electrochem. Solid-State Lett.*, 2007, **10**, A250–A254.

16 W. Zhang, P. Zhang, Z. Su and G. Wei, Synthesis and sensor applications of MoS_2-based nanocomposites, *Nanoscale*, 2015, **7**, 18364–18378.

17 M. R. Gao, Y. F. Xu, J. Jiang and S. H. Yu, Nanostructured metal chalcogenides: synthesis, modification, and applications in energy conversion and storage devices, *Chem. Soc. Rev.*, 2013, **42**, 2986–3017.

18 B. Radisavljevic, A. Radenovic, J. Brivio, V. Giacometti and A. Kis, Single-layer MoS_2 transistors, *Nat. Nanotechnol.*, 2011, **6**, 147–150.

19 C. Q. Feng, J. Li, H. Ma, R. Zeng, Z. P. Guo and H. K. Liu, Synthesis of molybdenum disulfide (MoS_2) for lithium ion battery applications, *Mater. Res. Bull.*, 2009, **44**, 1811–1815.

20 S. Z. Butler, S. M. Hollen, L. Y. Cao, Y. Cui, J. A. Gupta, H. R. Gutierrez, T. F. Heinz, S. S. Hong, J. X. Huang and A. F. Ismach, Progress, challenges, and opportunities in two-dimensional materials beyond graphene, *ACS Nano*, 2013, **7**, 2898–2926.

21 A. L. Elias, N. P. Lopez, A. C. Beltran, A. Berkdemir, R. T. Lv, S. M. Feng, A. D. Long, T. Hayashi, Y. A. Kim and M. Endo, Controlled synthesis and transfer of large-area WS_2 sheets: from single layer to few layers, *ACS Nano*, 2013, **7**, 5235–5242.

22 X. Wang, E. N. Kalali and D. Y. Wang, An *in situ* polymerization approach for functionalized MoS_2/nylon-6 nanocomposites with enhanced mechanical properties and thermal stability, *J. Mater. Chem. A*, 2015, **3**, 24112–24120.

23 O. Eksik, J. Gao, S. A. Shojaee, A. Thomas, P. Chow, S. F. Bartolucci, D. A. Lucca and N. Koratkar, Epoxy nanocomposites with two-dimensional transition metal dichalcogenide additives, *ACS Nano*, 2014, **8**, 5282–5289.

24 K. Chang and W. Chen, L-cysteine-assisted synthesis of layered MoS_2/graphene composites with excellent electrochemical performances for lithium ion batteries, *ACS Nano*, 2011, **5**, 4720–4728.

25 K. Chang and W. X. Chen, In situ synthesis of MoS_2/graphene nanosheet composites with extraordinarily high electrochemical performance for lithium ion batteries, *Chem. Commun.*, 2011, **47**, 4252–4254.

26 K. C. Batista Mancinelli, F. D. S. Lisboa, J. F. Soares, S. F. Zawadzki and F. Wypych, Poly(vinyl alcohol) nanocomposite films containing chemically exfoliated molybdenum disulfide, *Mater. Chem. Phys.*, 2013, **137**, 764–771.

27 N. Mirabal, P. Aguirre, M. Santa Ana, E. Benavente and G. Gonzáleza, Thermal stability and electrical conductivity in polyethers-molybdenum disulfide nanocomposites, *Electrochim. Acta*, 2003, **48**, 2123–2127.

28 I. Saada and R. Bissessur, Nanocomposite materials based on chitosan and molybdenum disulfide, *J. Mater. Sci.*, 2012, **47**, 5861–5866.

29 D. J. Late, B. Liu, H. Matte, C. Rao and V. P. Dravid, Rapid characterization of ultrathin layers of chalcogenides on SiO_2/Si substrates, *Adv. Funct. Mater.*, 2012, **22**, 1894–1905.

30 V. Štengl, J. Henych, M. Slušná and P. Ecorchard, Ultrasound exfoliation of inorganic analogues of graphene, *Nanoscale Res. Lett.*, 2014, **9**, 1–14.

31 K. P. Wang, J. Wang, J. T. Fan, M. Lotya, A. O'Neill, D. Fox, Y. Y. Feng, X. Y. Zhang, B. X. Jiang, Q. Z. Zhao, H. Z. Zhang, J. N. Coleman, L. Zhang and W. J. Blau, Ultrafast saturable absorption of two-dimensional MoS_2 nanosheets, *ACS Nano*, 2013, **7**, 9260–9267.

32 J. Q. Liu, Z. Y. Zeng, X. H. Cao, G. Lu, L. H. Wang, Q. L. Fan, W. Huang and H. Zhang, Preparation of MoS_2-polyvinylpyrrolidone nanocomposites for flexible nonvolatile rewritable memory devices with reduced graphene oxide electrodes, *Small*, 2012, **8**, 3517–3522.

33 A. Splendiani, L. Sun, Y. Zhang, T. Li, J. Kim, C. Y. Chim, G. Galli and F. Wang, Emerging photoluminescence in monolayer MoS 2, *Nano Lett.*, 2010, **10**, 1271–1275.

34 L. L. Tao, H. Long, B. Zhou, S. F. Yu, S. P. Lau, Y. Chai, K. H. Fung, Y. H. Tsang, J. Q. Yao and D. G. Xu, Preparation and characterization of few-layer MoS_2 nanosheets and their good nonlinear optical responses in the PMMA matrix, *Nanoscale*, 2014, **6**, 9713–9719.

35 G. S. Bang, K. W. Nam, J. Y. Kim, J. Shin, J. W. Choi and S. Y. Choi, Effective liquid-phase exfoliation and sodium ion battery application of MoS_2 nanosheets, *ACS Appl. Mater. Interfaces*, 2014, **6**, 7084–7089.

36 M. A. Ibrahem, T. W. Lan, J. K. Huang, Y. Y. Chen, K. H. Wei, L. J. Li and C. W. Chu, High quantity and quality few-layers transition metal disulfide nanosheets from wet-milling exfoliation, *RSC Adv.*, 2013, **3**, 13193–13202.

37 J. R. Potts, D. R. Dreyer, C. W. Bielawski and R. S. Ruoff, Graphene-based polymer nanocomposites, *Polymer*, 2011, **52**, 5–25.

38 Z. L. Yao, N. Braidy, G. A. Botton and A. Adronov, Polymerization from the surface of single-walled carbon nanotubes-preparation and characterization of nanocomposites, *J. Am. Chem. Soc.*, 2003, **125**, 16015–16024.

39 S. K. Kim, J. J. Wie, Q. Mahmooda and H. S. Park, Anomalous nanoinclusion effects of 2D MoS_2 and WS_2 nanosheets on the mechanical stiffness of polymer nanocomposites, *Nanoscale*, 2014, **6**, 7430–7435.

40 M. A. Rafiee, J. Rafiee, Z. Wang, H. H. Song, Z. Z. Yu and N. Koratkar, Enhanced mechanical properties of nano-composites at low graphene content, *ACS Nano*, 2009, **3**, 3884–3890.

41 A. S. Zerda and A. J. Lesser, Intercalated clay nanocomposites: Morphology, mechanics, and fracture behavior, *J. Polym. Sci., Part B: Polym. Phys.*, 2001, **39**, 1137–1146.

42 K. Wang, L. Chen, J. S. Wu, M. L. Toh, C. B. He and A. F. Yee, Epoxy nanocomposites with highly exfoliated clay: Mechanical properties and fracture mechanisms, *Macromolecules*, 2005, **38**, 788–800.

43 N. Illy, S. Benyahya, N. Durand, R. Auvergne, S. Caillol, G. David and B. Boutevin, The influence of formulation and processing parameters on the thermal properties of a chitosan–epoxy prepolymer system, *Polym. Int.*, 2014, **63**, 420–426.

44 S. Vadukumpully, J. Paul, N. Mahanta and S. Valiyaveettil, Flexible conductive graphene/poly(vinyl chloride) composite thin films with high mechanical strength and thermal stability, *Carbon*, 2011, **49**, 198–205.

45 H. Alamri and I. M. Low, Effect of water absorption on the mechanical properties of nano-filler reinforced epoxy nanocomposites, *Mater. Des.*, 2012, **42**, 214–222.

46 Y. X. Zhou, M. I. Jeelani and S. Jeelani, Development of photo micrograph method to characterize dispersion of CNT in epoxy, *Mater. Sci. Eng., A*, 2009, **506**, 39–44.

47 M. Monti, M. Rallini, D. Puglia, L. Peponi, L. Torre and J. M. Kenny, Morphology and electrical properties of graphene-epoxy nanocomposites obtained by different solvent assisted processing methods, *Composites, Part A*, 2013, **46**, 166–172.

48 L. C. Tang, Y. J. Wan, D. Yan, Y. B. Pei, L. Zhao, Y. B. Li, L. B. Wu, J. X. Jiang and G. Q. Lai, The effect of graphene dispersion on the mechanical properties of graphene/epoxy composites, *Carbon*, 2013, **60**, 16–27.

49 D. Wang, K. Q. Zhou, W. Yang, W. Y. Xing, Y. Hu and X. L. Gong, Surface modification of graphene with layered molybdenum disulfide and their synergistic reinforcement on reducing fire hazards of epoxy resins, *Ind. Eng. Chem. Res.*, 2013, **52**, 17882–17890.

50 M. C. Hsiao, S. H. Liao, Y. F. Lin, C. A. Wang, N. W. Pu, H. M. Tsai and C. C. M. Ma, Preparation and characterization of polypropylene-graft-thermally reduced graphite oxide with an improved compatibility with polypropylene-based nanocomposite, *Nanoscale*, 2011, **3**, 1516–1522.

51 J. J. Liang, Y. Huang, L. Zhang, Y. Wang, Y. F. Ma, T. Y. Guo and Y. S. Chen, Molecular-level dispersion of graphene into poly(vinyl alcohol) and effective reinforcement of their nanocomposites, *Adv. Funct. Mater.*, 2009, **19**, 2297–2302.

52 X. L. Ji, J. K. Jing, W. Jiang and B. Z. Jiang, Tensile modulus of polymer nanocomposites, *Polym. Eng. Sci.*, 2002, **42**, 983–993.

53 B. Q. Chen and J. R. G. Evans, Nominal and effective volume fractions in polymer-clay nanocomposites, *Macromolecules*, 2006, **39**, 1790–1796.